

Superhigh-sensitivity photothermal monitoring of individual cell response to antitumor drug

Vladimir P. Zharov

Valentin Galitovskiy

University of Arkansas for Medical Sciences
Philips Classic Laser Laboratories
Little Rock, Arkansas 72205-7199

Christopher S. Lyle

Timothy C. Chambers

University of Arkansas for Medical Sciences
Department of Biochemistry and Molecular Biology
Little Rock, Arkansas 72205-7199

Abstract. We describe and explore the capability of a photothermal (PT) assay with modified schematics for highly sensitive detection of individual cell response to antitumor drug impact *in vitro*. Specifically, we used the nonlinear differential PT test to measure distinctive changes of specific PT parameters after exposure of KB3 carcinoma cells to the antitumor drug vinblastine in the broad concentration range of 10^{-10} to 300 nM. Verification of the PT assay was performed by comparison with multidrug-resistant cells and comparison with conventional assays evaluating cell viability, cytochrome c release, apoptosis induction, and cell size. We demonstrate that this system is capable of detecting drug-induced signals at a concentration threshold sensitivity at least seven orders of magnitude better than existing assays. We anticipate that this technique may serve as a convenient and rapid analytical tool to evaluate the presence of intracellular drug, with applications in high throughput screening assays and for studying drug uptake and distribution in more complex biological or clinical samples. © 2006 Society of Photo-Optical Instrumentation Engineers. [DOI: 10.1117/1.2405349]

Keywords: laser; imaging; photothermal effects; cancer cells; drug; vinblastine; apoptosis; cytotoxicity; mitochondria.

Paper 06036R received Feb. 24, 2006; revised manuscript received Jun. 21, 2006; accepted for publication Jul. 13, 2006; published online Dec. 21, 2006.

1 Introduction

Many systems have been developed to test general and specific drug toxicity at the cellular level.¹⁻⁴ In particular, development of new cancer chemotherapeutic agents (or improvement of conventional ones) requires rapid estimation of efficiency, dose optimization, and specificity, and ideally takes into account individual patient tumor drug resistance at particular stages of progression. However, most existing cytotoxicity assays, such as standard cell viability and apoptosis assays, are not suitable for such tasks because they are time-consuming, relatively complex, and expensive.⁵⁻¹³ Several optical assays that have been developed to overcome these problems have shown promise. In absorption (transmittance) spectroscopy, drug action is evaluated through changes of attenuation in optical radiation resulting from corresponding changes in endogenous intracellular absorbing structures, for example, changes in the redox state of cytochrome c by cyanide.¹⁴ A common problem of this technique, however, is its relatively low absorption sensitivity due to the short optical path of light in cells. Phase contrast and differential-interference contrast microscopy provide information about drug action by monitoring changes in the cellular fine-refractive structures, for example, metabolic and toxic-related changes in mitochondrial shape and size.^{15,16} Although this technique yields more specific information on cellular

changes, its sensitivity is only one order of magnitude greater than conventional cytotoxicity tests. Currently, fluorescence-labeling scanning microscopy and flow cytometry provide the most powerful tools for observing and quantitating metabolic, physiologic, and morphologic parameters in single cells after drug treatment.^{17,18} Despite their appeal, these techniques have limitations due to photobleaching effects and the escape of fluorescent indicators through diffusion. Moreover, growing evidence suggests that these indicators may seriously distort genuine cell-drug interactions through unwanted indicator-cell and indicator-drug interactions.^{19,20} More recently, nonresonant Raman spectroscopy was used to image DNA and protein redistribution during paclitaxel-induced apoptosis in single HeLa cells.²¹ However, a relatively weak scattering phenomenon limited this technique to studying dense biological structures only, such as nuclei. Another technique, optical scattering imaging, is capable of monitoring calcium-induced alterations in mitochondrial morphology, as verified by parallel fluorescent and differential-interference contrast microscopy.²² These techniques do not require a staining procedure, making them promising candidates for further development.

Because most cellular structures are not fluorescent or are weakly fluorescent, most absorbed light energy is transformed through nonradiative relaxation in the form of heat, which can be detected with photothermal (PT) techniques.^{23,24} For non-fluorescent samples, this technique provides the highest absorption sensitivities (approximately five orders of magnitude

Address all correspondence to: Vladimir P. Zharov, University of Arkansas for Medical Sciences, Philips Classic Laser Laboratories, Mail Slot 543, 4301 W. Markham St., Little Rock, AR 72205-7199; tel: 501-686-6140; E-mail: ZharovVladimirP@uams.edu

better than transmission spectroscopy) and allows evaluation of very low concentrations of biomolecules, without labeling, with a sensitivity comparable to that of laser fluorescence methods that require labeling.^{25,26} Preliminary studies have demonstrated PT responses from cells subjected to different environmental impacts including photodynamic effects,^{27,28} the influence of drugs,²⁹ and chemical and radiation inducers of apoptosis.^{30–35} In particular, we have recently developed and experimentally verified the nanocluster model of the PT assay with the use of a laser-induced microbubble around endogenous (e.g., cytochrome c in mitochondria^{24,36}) or exogenous (e.g., bioconjugated gold nanoparticles^{37,38}) absorbers as indicators of environmental and therapeutic impact (e.g., radiation).³⁵ However, the PT data were not correlated directly with toxicological and apoptotic effects or verified with conventional assays over a large concentration range; the underlying mechanisms were not investigated; the data were mostly obtained with relatively poor resolution (0.7 to 1 μm); and threshold sensitivity was not estimated. In the present study, we demonstrate the remarkable sensitivity and utility of the PT technique as a probe for antitumor drug action. We demonstrate that this system is capable of detecting drug-induced cell alteration at a concentration threshold sensitivity at least seven orders of magnitude better than existing assays. We anticipate that this technique may serve as a convenient and rapid analytical tool to evaluate the presence of an intracellular drug, with applications in high throughput screening assays and for studying drug uptake and distribution in more complex biological or clinical samples.

2 Methods

2.1 Principle and Schematics of the PT Technique

The irradiation of a single cell with a laser pump pulse leads to an increase in the temperature of local cellular absorbing non- or weakly fluorescent structures. This temperature increase at the short laser pulse, when heat diffusion from the heated area is negligible during the pulse, depends upon the coefficient absorption, laser pulse energy, and the thermodynamic parameters of the absorbing target (e.g., the density and the heat capacity).²⁴ For typical laser fluence of 0.1 to 10 J/cm^2 in the visible spectral range for cells with different absorbing profiles, local temperature ranged from 0.1 to 1 °C to 100 to 300 °C,²⁴ thus providing a broad spectrum action from noninvasive to invasive, respectively, with manifestation of bubble formation phenomena (typically at temperature range of 150 to 250 °C).³⁴ In turn, the temperature distribution is transformed into refraction distribution, which can be detected with a second probe pulse.²⁴ The PT response, which is proportional to temperature changes in pulse mode, demonstrates a high initial peak due to fast (nanosecond scale) heating of the absorbing structure and a much longer (microsecond scale) exponential tail corresponding to the cooling of the cell as a whole.

The PT-response amplitude and temporal shape depend on several cellular parameters, such as local coefficient absorption, characteristic relaxation times, thermodynamics, and especially, geometric parameters. All of these may be influenced by drug impact. In particular, the PT response demonstrated high sensitivity to shrinking (or swelling) of the intracellular absorbing structures as well as the cell as a whole, especially

in nonlinear mode with manifestation of microbubble formation around the most strongly overheated absorbing zones.^{33,34} The reversible shrinking of the cell as a whole, and especially that of subcellular organelles, is typically related to metabolic responses to low drug doses or early apoptosis, whereas swelling phenomena are associated with necrosis.^{39–43} For example, if the laser-induced temperature before drug impact is close to the phase transition threshold (e.g., related with evaporation), even a small drug-induced shrinking of absorbing zones will lead to an increase of local absorption and hence, to local temperature that can be accompanied by the sudden appearance of nonlinear phenomena (i.e., bubble formation). This feature makes the PT method, in both linear and especially, nonlinear modes, supersensitive to small nanomorphological cell modifications unachievable with other assays. In particular, according to the nanocluster model,³⁴ the spatial relocation of molecules in nanoclusters within just 5 to 10 nm leads to a change of local absorption within a few percent that can be detected with the PT assay.

As an improvement to previous research applications,²⁹ we developed a new PT time-resolved microscope and spectrometer with advanced thermolens imaging on the technical platform of the Olympus BX51 microscope (Olympus, Melville, New York) (Fig. 1). Briefly, in this system, a single cell is irradiated with a short pump laser pulse, generated by a tunable optical parametric oscillator (OPO) with the following parameters: spectral tuning range, 420 to 900 nm; pulse width, 8 ns; pulse energy, 0.1 to 1000 μJ (average fluence 0.02 to 200 J/cm^2) (Lotis Ltd., Minsk, Belarus). For time-resolved monitoring of laser-induced local thermal effects, including bubble formation around overheated absorbing zones, a conventional dual-pump-probe thermolens mode was applied^{23,24} with a new optical configuration. In one-channel mode, laser-induced temperature-dependent local variations of the refractive index into cells causes a focusing or defocusing of a collinear, continuous-wave stabilized, He-Ne laser probe beam (wavelength 633 nm and power 1.4 mW) (Model 117A, Spectra-Physics Inc., Mountain View, California). The resultant reduction of laser intensity at the beam center is recorded by a photodiode (C5658, Hamamatsu Corp., Bridgewater, New Jersey) with a pinhole (0.3-mm diameter) and an oscilloscope (TDS 3032B, Tektronix Inc., Richardson, Texas). The pump and probe beam diameter are adjustable (range 20 to 30 μm and 15 to 25 μm , respectively) by an axial moving condenser, or by the use of microobjectives with magnification ranges of 4 \times , 10 \times , 20 \times , 60 \times , or 100 \times . Because relatively large laser beams cover the whole cells, the PT thermolens response is proportional to the average absorption within cells with more profound influence of absorption from the cell center near the beam axis. The imaging with these schematics can be realized by scanning more strongly focused laser beams across cells.³⁰ However, because it is a time-consuming procedure, we developed a new, more rapid mode that required just one pump pulse.

The PT imaging in this mode is created by irradiating a cell with the same pump beam, and detecting the defocusing effects of a second, collinear laser probe pulse (Raman shifter, 639 nm; pulse width, 13 ns; pulse energy, 2 nJ) using a AE-260E charge-coupled device (CCD) camera (512 \times 512 pixels and pixel size of 20 μm ; Apogee Inc., Santa

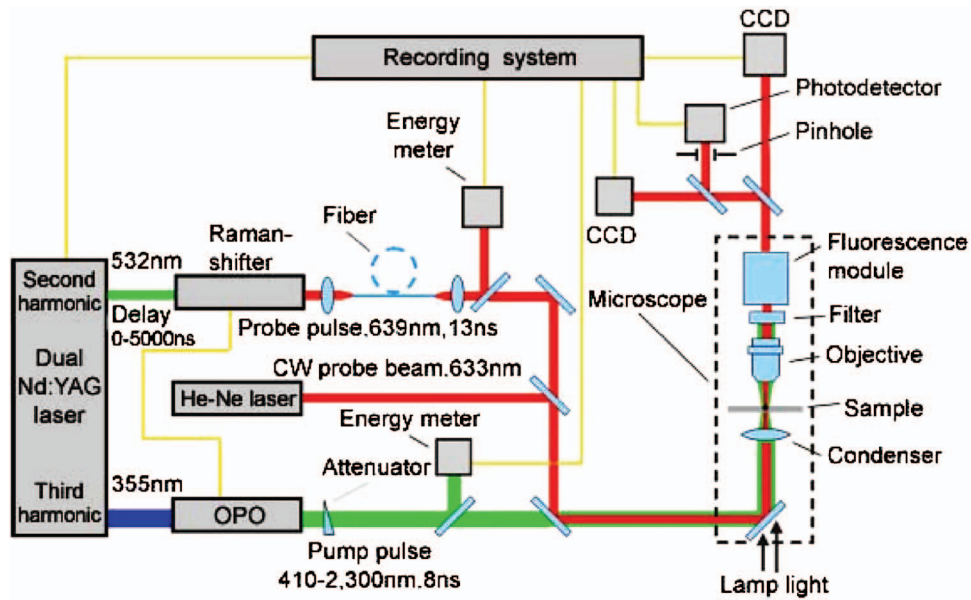


Fig. 1 Schematics of advanced photothermal assay. OPO—optical parametric oscillator; CCD—charge-coupled device.

Monica, California). In this mode, each CCD pixel with its margin plays the role of a single photodetector within a pinhole, respectively, as in the one-channeled thermolens mode.^{44,45} Thus, a wide-field CCD-based PT microscope is equivalent to a multichanneled thermolens imaging system in which the channel number is determined by the number of pixels. This schematic satisfies the requirement for the creation of an adequate image because there is a correlation in the thermolens technique between optical fields immediately after the object in the sample plane and the intensity distribution in the detected area (i.e., in the CCD pixel's plane). The experimental verification of this imaging was performed by

selecting a local area within the cross section of laser beam with a pinhole, and then detecting defocusing effects within this area with just one or several CCD pixel selected with a second pinhole. We found that the change of PT signal amplitude from one pixel was similar to PT response detected with the conventional photodetector with pinhole (data not shown).

The entire PT image acquisition procedure included illumination of the cells with three pulses: (1) an initial probe pulse followed by (2) a 0.1-s delay to the pump pulse and then (3) a second probe pulse with a tunable delay (0 to 5000 ns) to the pump pulse. The calculation difference

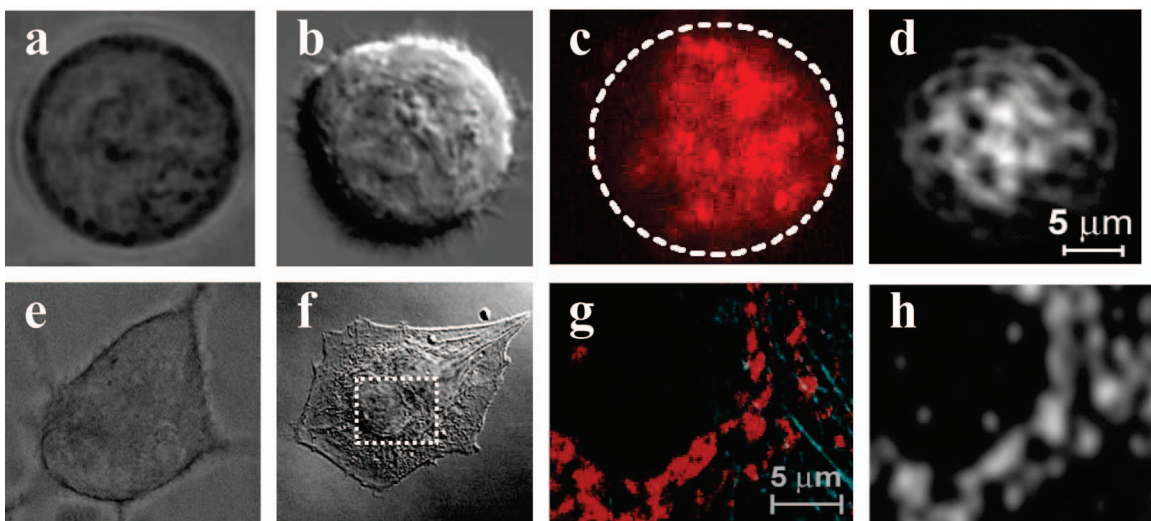


Fig. 2 Images of KB3 cells in suspension (a) to (d) and on adherent surface (e) to (h): (a), (e) transmitted; (b), (f) phase contrast; (c), (g) fluorescent with MitoTracker Red Fluorescence; and (d), (h) PT images. Images in panels (g) and (h) show enlarged versions of the fragment of cell near nucleus marked by the dash line in panel (f). PT images (d) and (h) were obtained at pump laser parameters: wavelength, 525 nm; pulse width, 8 ns; energy, 20 μ J; probe time delay, 10 ns. The images (g) and (h) were obtained from the same cells. PT images of KB3 cells in suspension (d) obtained with conventional PT phase contrast imaging with a 20 \times objective (Ref. 24), while PT image on substrate was obtained with new PT thermolens imaging with magnification 60 \times , and resolution around 400 nm (Refs. 44 and 45).

between the two probe images, with normalization of each pixel on laser pulse energies, allowed acquisition of a PT thermolens image in analogy to PT phase contrast images.^{24,46} These both depend on cell absorption only without the possible influences of phase distortion on the probe beam, natural refractive heterogeneities of the sample, light scattering effects, and possible variation of the probe and pump laser energy. The pump and probes beams have a stable, smooth Gaussian-like intensity profile controlled with the CCD camera.²⁴ As a result, formation of a PT image requires just one pump pulse with a relatively broad beam diameter (e.g., 30 μm for pump beam, and 20 μm for probe beam in most experiments) covering an entire single cell of typical diameter around 14 to 18 μm . Thus, time-consuming scanning with a strongly focused laser beam across each individual cell, as in conventional laser thermolens imaging, was unnecessary. The influence of a Gaussian-like beam profile on cell image quality was reduced by use of only the central part of the laser beam with diameter larger than cell size and algorithm of the subtraction of two probe images (see above). With this schematic, a spatial resolution is determined by the microscope objective aperture rather than by the laser beam diameter (approximately 700 nm at 20 \times , and 300 nm at 100 \times). Due to the short duration of the laser pulse (8 ns), the influence of heat diffusion from laser-heated cellular absorbing structures on optical resolution is negligible.⁴⁵ Measurement of PT responses at different pump wavelengths permitted the acquisition of PT spectrum from single cells and their absorbing structures.²⁴ The monitoring of changes in PT response amplitude and temporal shape at different laser pump energies allowed examination of laser-induced nonlinear phenomena (e.g., bubble formation) and cell photodamage threshold.⁴⁷

2.2 Cell Culture and Drug Treatment

For verification of the PT assay, we examined KB3 cells treated with the microtubule inhibitor vinblastine, a well-established model of drug-cell interaction that induces apoptosis under lethal conditions.^{48–50} KB3 cells were maintained in Dulbecco's modified Eagle's medium supplemented with 10% fetal calf serum, 50 U/mL of penicillin, 50 $\mu\text{g}/\text{mL}$ of streptomycin, and 5 mM of L-glutamine at 37°C and 5% CO₂. Cell culture reagents were obtained from Life Technologies (Carlsbad, California). Cells were seeded in 60-mm tissue culture dishes, grown overnight, and then treated with vinblastine (Sigma, St. Louis, Missouri) by diluting the drug 1:1000 in growth media at the appropriate concentration. Controls received vehicle [0.1% dimethylsulfoxide (DMSO)] alone. Cells were washed three times with 4 mL of phosphate buffered saline. The cells were either studied in suspension in sealed chambers (S-24737; Molecular Probes, Oregon) at a concentration of 10⁶ cells/mL or fixed on a microscope slide. KB-V1 cells, which are vinblastine-resistant, were maintained in the same media containing 1 $\mu\text{g}/\text{mL}$ of vinblastine and were described previously.⁵¹

2.3 Cell Viability and Apoptosis Assays

Inhibition of cell proliferation by vinblastine was measured by the 3-(4,5-dimethylthiazol-2-yl)-2,5-diphenyltetrazolium bromide (MTT) assay.⁴⁸ Cells (2000 per well) were plated in 96-well dishes, and after 24 h, the medium was replaced with

fresh medium containing either vinblastine (0.1 to 100 nM in 0.1% DMSO) or vehicle alone and treated for 48 h. All treatments were performed in triplicate, and viability was expressed as a percentage of the untreated controls. Detection of cytosolic cytochrome c was determined by subcellular fractionation and immunoblotting as described previously.⁵⁰ Cleavage of poly (adenosine diphosphate-ribose) polymerase (PARP), as an apoptotic marker, was examined by immunoblotting as described previously.⁵⁰

2.4 Confocal Laser Scanning Microscopy

KB3 cells were cultured in six-well plates and treated with different concentrations of vinblastine ranging from 10⁻¹⁰ to 10 nM. For the analysis of mitochondria, cells were treated with 0.1 μM of MitoTracker Red CMXRos (Molecular Probes) for 30 min before fixation. Cells were fixed with 3% paraformaldehyde and permeabilized with 0.2% Triton X100. For cytochrome c staining, cells were treated with anti-cytochrome c antibody according to manufacturer's instructions (Pharmingen, San Diego, California). Anticytochrome c treated cells were visualized with Oregon Green-conjugated second antibody (Molecular Probes). Fluorescence was observed using a Zeiss LSM 410 confocal laser scanning microscope. Cell size was measured in transmission mode, with a minimum of 150 cells for each condition. Mitochondria size was measured similarly.

3 Results

3.1 Photothermal Imaging of Cells

PT assay (imaging) is a relatively new technique, and we first determined whether the response would be optimized using suspension versus adherent cells and to directly compare this new technique with conventional imaging techniques. Figure 2 presents PT images compared to transmission, phase contrast, and fluorescence, of a single KB3 cell, either in suspension [Figs. 2(a)–2(d)] or on substrate [Figs. 2(e)–2(h)]. It is evident that the PT assay permits imaging of tiny local absorbing cellular structures [Figs. 2(d) and 2(h)] that are invisible by conventional transmission techniques [Figs. 2(a) and 2(e)] due to its low absorption sensitivity. The quality of the PT image was superior when cells were visualized on substrate rather than in suspension, and subcellular structures and their boundaries were more clearly observed. For example, the nuclear region was more clearly defined with adherent cells [Fig. 2(h)] compared to suspension cells [Fig. 2(d)]. Note that the nucleus itself does not absorb in the spectral range used, and with adherent cells, the nuclear region is less obscured by mitochondria. When cells were labeled with MitoTracker Red [Fig. 2(g)], the fluorescent image obtained had a pattern very similar to that of the PT image, suggesting that the main absorbing target of PT is located in the mitochondria. Additional measurements of the PT spectra of individual local zones in PT images in Fig. 2(h) obtained at different wavelengths of the pump laser revealed a good correlation with the conventional spectrum of cytochrome c, at least in the spectral range of ~530 to 560 nm (data not shown, see method details in Ref. 24).

High quality PT images suitable for accurate quantitation and identification of cellular absorbing components were best obtained with adherent cells versus suspension cells [Fig.

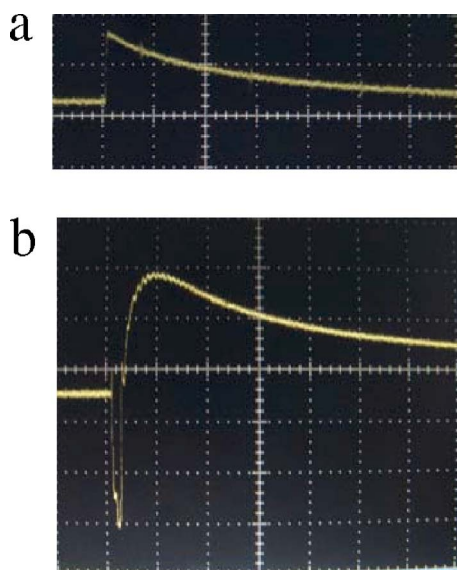


Fig. 3 Typical temporal shape of integrated PT responses from a KB3 cell in suspension, at different laser energy. Laser energy and amplitude/time scale: (a) $20 \mu\text{J}$, $50 \text{ mV}/10 \mu\text{s}/\text{division}$; and (b) $160 \mu\text{J}$, $200 \text{ mV}/10 \mu\text{s}/\text{division}$.

2(d)]. However, data collection was relatively time-consuming when individual cells were analyzed. On the other hand, cells in suspension were more convenient for rapid monitoring, especially in flow cytometry mode,^{36,52,53} and still provided quantitative concentration-dependent PT responses over a wide concentration range.³⁴ We therefore further investigated this approach to monitor integrated PT responses from single cells in suspension.

3.2 Characteristics of Cellular Photothermal Response

We next explored the potential of the PT technique to provide quantitative data of the intracellular effects of cytotoxic drugs. To achieve this, we first measured the time-resolved PT response amplitude from single cells in suspension. In untreated KB3 cells, at a relatively low laser fluence ($<8 \text{ J}/\text{cm}^2$) not causing cell photodamage, a high initial peak PT response due to fast heating was observed, followed by slow exponential cooling resulting from heat diffusion into the surrounding solution [Fig. 3(a)]. This PT response is similar to that observed in other cell lines.^{24,31–37} The averaged thermal relaxation time^{24,34} τ_T was determined to be $42 \pm 5 \mu\text{s}$ with an estimated temperature elevation of $6 \pm 0.7^\circ\text{C}$. This relaxation time corresponds to a cell size of $16 \mu\text{m}$ (assuming a spherical cell), close to the measured cell diameter of 17 to $20 \mu\text{m}$ (see Fig. 7). The PT response amplitude increased with pulse energy until local temperatures reached the evaporation thresholds (~ 150 to 220°C).³⁴ At these energy levels, a sharp decrease (negative peak) was observed, followed by an increase, and then a gradual decay as before [Fig. 3(b)]. The shape of these curves is related to microbubble formation around the local absorbing structures, with the negative peak created by rapid bubble expansion and collapse with changes in local refractive index, light scattering and temperature.⁴⁷ The appearance of the bubbles and their precise life span, ranging from

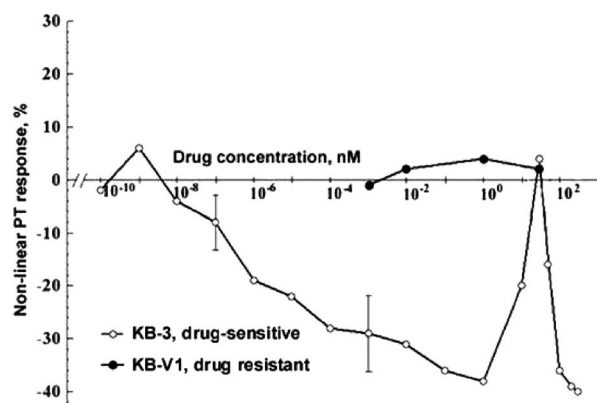


Fig. 4 Differential nonlinear PT response ($\delta\Delta_{NL}$, as defined in text) from drug-sensitive KB3 and multidrug-resistant KB-V1 cells as a function of vinblastine concentration. Cells were treated with the indicated concentration of vinblastine for 24 h. KB3 cells, open symbols; KB-V1 cells, closed symbols. Laser energy (fluence) was $110 \mu\text{J}/\text{cm}^2$, wavelength, 525 nm .

0.2 to $10 \mu\text{s}$, is strictly dependent on the size of the endogenous cellular absorbing structures, providing a very sensitive method to examine the effects of agents that cause such changes. PT responses without [i.e., Fig. 3(a)] or with negative components [i.e., Fig. 3(b)] were referred to as linear or nonlinear PT responses, respectively.

3.3 Quantitation of Photothermal Response as a Function of Drug Concentration

In a method similar to that used in laser viability tests,³² we measured the percentage of linear and nonlinear PT responses, which were produced after irradiation of single cells with one laser pulse, as described in Sec. 2. The experimental results were used to calculate a ratio: $\delta_{NL} = N_{NL}/N \times 100\%$, where N is the total number of PT responses after a one-time irradiation of each cell with just one laser pulse, and $N = N_L + N_{NL}$, and where N_L and N_{NL} are the number of linear and nonlinear PT responses, respectively. The total number of irradiated cells was 100, and all experiments were performed three times under the same conditions. Thus, the change of the nonlinear PT responses was used here as an indicator of drug-induced change in the local absorption. The results are presented as differences in the percent of the number of nonlinear PT responses between drug-treated and control cells, that is, as $\Delta\delta_{NL} = (\delta_{NL})_{drug} - (\delta_{NL})_{cont}$. To distinguish from the laser load test,³² we named this modified approach the nonlinear differential PT test (see details in Ref. 34). By measurement of differential nonlinear PT responses at different laser energies at a specific wavelength (525 nm) and with a constant drug dose (1 nM , 24 h treatment), the energy range, which provided maximum PT response, was determined to be $110 \pm 25 \mu\text{J}$ (fluence $22 \pm 5 \text{ J}/\text{cm}^2$).

To demonstrate the power and potential of this technique to examine drug impact, we measured differential nonlinear PT responses $\Delta\delta_{NL}$ in KB3 cells as a function of vinblastine treatment over a wide concentration range (Fig. 4). We first examined drug-sensitive KB3 cells treated for 24 h, at vinblastine concentrations of 10^{-10} to 300 nM . A small increase within experimental error was observed at very low vinblas-

tine concentrations of 10^{-9} nM. With concentration increase, the PT response decreased in a dose-dependent fashion, reaching a minimum at around 1 nM. At higher concentrations and within a narrow concentration range of 10 to 50 nM, the PT response rapidly returned to the level of control cells and rapidly decreased again. As shown in Sec. 4, these more abrupt changes at higher concentrations corresponded to lethal drug doses. This profile was highly reproducible and was observed in five independent experiments.

To further investigate the nature of the PT signal with respect to the interaction of vinblastine with internal cellular structures, we used the multidrug-resistant KB-V1 cell line. KB-V1 cells are highly drug-resistant and exhibit a 50% inhibitory concentration (IC_{50}) for vinblastine of $5 \mu\text{M}$ (versus KB3 cells with IC_{50} of 0.8 nM).⁵¹ The resistance is due to P-glycoprotein-mediated drug efflux, thus KB-V1 cells do not accumulate vinblastine internally. The PT response of KB-V1 cells was relatively unchanged in the range of 10^{-3} to 30 nM of vinblastine (Fig. 4). These results indicate that the robust PT response in KB3 cells is due mostly to drug impact on intracellular components.

3.4 Comparison with Conventional Cytotoxicity Assays

MTT viability assays were performed with KB3 cells treated with vinblastine for 48 h. Concentrations up to 0.3 nM had no observable effect on viability, whereas a concentration of 1 nM was growth inhibitory, with essentially no cell survival at higher concentrations [Fig. 5(a)]. An IC_{50} value of 0.8 nM was derived from these data. It is evident that the maximum negative response in the PT assay (Fig. 4) closely corresponded to this IC_{50} value, and that lethal conditions (>1 nM) correspond to the most dramatic changes in the PT response curve. Lethal concentrations of vinblastine also caused cytochrome c release from mitochondria to the cytosol [Fig. 5(b)]. To confirm that vinblastine induced apoptotic cell death at these higher concentrations, cleavage of PARP was examined by immunoblotting. PARP was cleaved into its characteristic truncated form (85 kDa) at vinblastine concentrations of 1 nM and higher, confirming an apoptotic form of cell death [Fig. 5(c)]. Cytochrome c release and PARP cleavage were only evident at lethal vinblastine concentrations and were not detected at concentrations of 0.3 nM or lower. Thus, the standard tests of cell viability and cell apoptosis depicted in Figs. 5(a)–5(c) were much less sensitive than the PT response. For example, a PT response was readily detectable after 24-h treatment with 10^{-7} nM of vinblastine, while concentrations approaching 1 nM and above were required to observe changes using conventional viability and apoptotic assays.

3.5 Relationship to Mitochondrial and Cell Size

To further document and confirm a role of mitochondria and cytochrome c release in cell death induced by vinblastine, and to relate PT responses to such changes, we undertook fluorescent imaging of mitochondria and cytochrome c, as described in Sec. 2. Figure 6(a)–(c) shows images of mitochondria obtained from control cells and cells treated with 1 or 10 nM of vinblastine for 24 h. Mitochondria were either spherical or elongated, with spherical mitochondria having a mean diam-

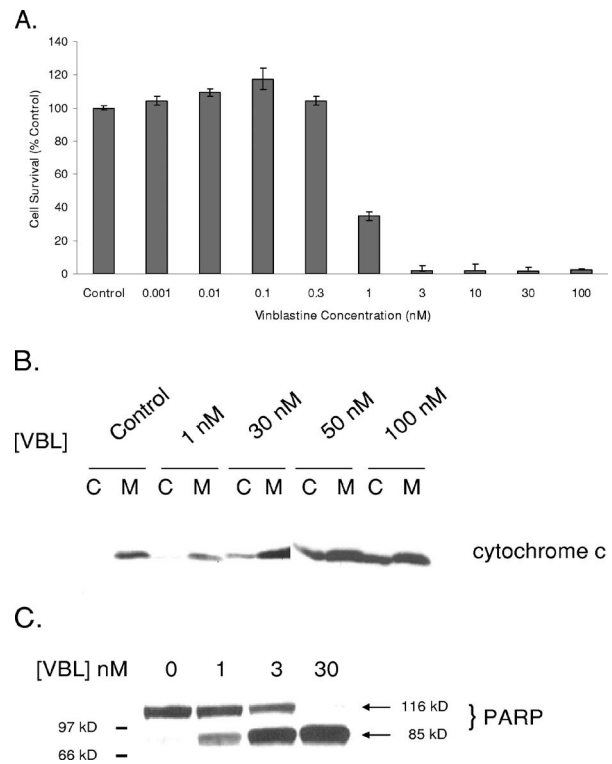


Fig. 5 Conventional cytotoxicity tests of influence of vinblastine on KB3 cells. (a) Inhibition of cell viability. Cells were treated with the indicated concentration of vinblastine and cell viability determined by MTT assay after 48 h. Values are the means of triplicate assays and are expressed as mean \pm standard deviation relative to control (untreated) cells. Essentially identical results have been obtained in two repeats of this experiment. (b) Cytochrome c release. KB3 cells were either untreated or treated with the indicated concentration of vinblastine for 48 h, and cytosolic (C) or mitochondrial (M) fractions were subjected to immunoblotting for cytochrome c. (c) PARP cleavage. KB3 cells were treated with the indicated concentration of vinblastine for 48 h and cell extracts subjected to immunoblotting for PARP. The uncleaved (116 kDa) and cleaved species (85 kDa) are indicated.

eter of $0.80 \pm 0.15 \mu\text{M}$, as determined by high-resolution transmission microscopy. Comparison of the average diameter of similarly shaped mitochondria indicated an increase in diameter of $45 \pm 12\%$ at 1 nM of vinblastine [Fig. 6(b)] compared to control cells [Fig. 6(a)]. However, mitochondrial swelling was reversed at a concentration of 10 nM of vinblastine [Fig. 6(c)], with average mitochondrial diameters more similar to control cells. As the first observation of this phenomenon, we repeated the experiments with simultaneous imaging of cytochrome c. In control cells, the distribution pattern of cytochrome c matched that of the mitochondria [Fig. 7(a) and 7(b)]. At 1 nM of vinblastine, corresponding to the maximum negative PT response, we observed again mitochondrial swelling without cytochrome c release [Fig. 7(c) and 7(d)]. At 10 nM of vinblastine, corresponding to large changes in the PT response, we observed slight mitochondrial shrinkage and initial signs of cytosolic cytochrome c [Fig. 7(e) and 7(f)].

Finally, we sought to determine whether there was a relationship between the PT responses and cell size at different drug concentrations. The average diameter of cells in suspen-

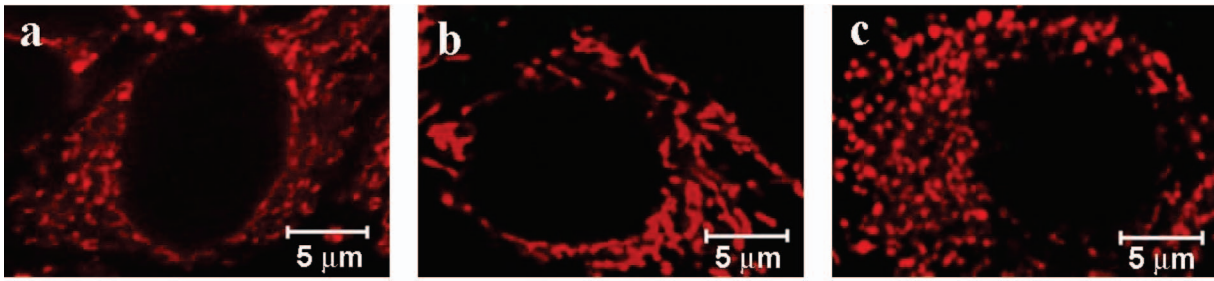


Fig. 6 Fluorescent images of KB3 cells on substrate after staining with MitoTracker Red to visualize mitochondria. Panel (a) shows the control, untreated cells; panel (b) shows 1 nM of vinblastine at 24 h; and panel (c) shows 10 nM of vinblastine at 24 h.

sion was monitored with high-resolution transmission microscopy as a function of drug dose and incubation time. Under each condition, 150 cells were analyzed. As shown in Fig. 8, cell size underwent changes as the concentration of vinblastine increased. Initially, in the range 10^{-6} to 10^{-2} nM, there was a slight increase in the size, followed by a return to con-

trol value at around 1 nM. At higher concentrations, particularly within the narrow range of 1 to 50 nM of vinblastine, there was a more dramatic increase in cell size of approximately 30%. Thus, drug-induced changes in cell size occurred more prominently at vinblastine concentrations higher than that which caused mitochondrial swelling.

4 Discussion

In this paper, we have described an application of a laser-based PT method (assay) for testing drug impact at a single cell level *in vitro*. Specifically, we studied the distinctive changes of PT parameters after exposure of KB3 carcinoma cells to the antitumor drug vinblastine in a broad concentration range of 10^{-10} to 300 nM. We demonstrated that this system has many advantages over conventional techniques including high sensitivity, simplicity, and rapidity, with the ability to provide quantitative information on drug impact. For example, a PT signal is readily obtained after exposure of cells to 10^{-7} nM of vinblastine (Fig. 4), some six to seven orders of magnitude lower than conventional viability assays (Fig. 5). Further, this information is obtained with minimal cell preparation and with no requirement for labeling or staining of cells. In particular, the PT assay only requires about 5 to 10 μ l of cell suspension. The minimum number of cells for PT assay (usually, 100 to 500 cells) depends on the cell absorbing structure heterogeneity and the dependence of PT

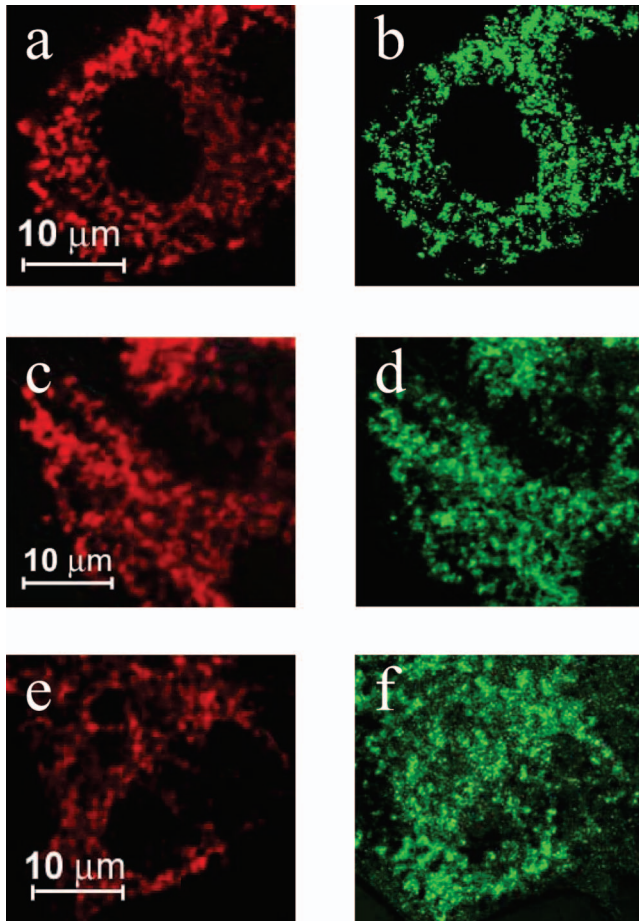


Fig. 7 Fluorescent images of KB3 cells showing mitochondria and cytochrome c distribution. The images (a), (c), (e) were obtained from different cells with MitoTracker Red; panels (b), (d), (f) show immunofluorescent localization of cytochrome c visualized with Oregon Green. Panels (a), (b) show untreated control cells; panels (c), (d) show the same cells treated with 1 nM of vinblastine at 24 h; and panels (e), (f) show the same cells treated with 10 nM of vinblastine at 24 h.

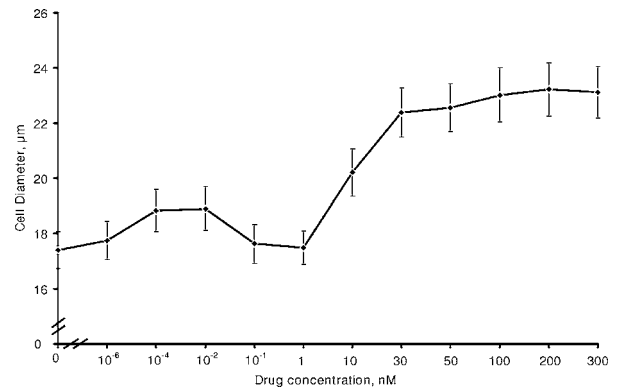


Fig. 8 Effect of vinblastine on cell size. Cells were treated for 24 h with the indicated concentration of vinblastine and cells were processed for measurement of cell diameter as described in Sec. 2. For each point, a minimum of 150 cells were used, with data expressed as mean \pm standard deviation.

response on this heterogeneity. In addition, data acquisition is extremely rapid, within minutes, with PT information from a single cell obtained during a one laser pulse. To our knowledge, there is no existing assay that combines these attributes of sensitivity, rapidity, and convenience.

Specifically, the PT response profile from vinblastine-treated KB3 cells exhibited specific features that were highly reproducible within the PT assay accuracy ($\sim 7\%$). In the range 10^{-8} to 0.3 nM of vinblastine, the nonlinear PT response had a magnitude that was dose-dependent with respect to drug concentration. In this very low drug concentration range, the PT response was robust, whereas more conventional assays, including those measuring cell viability, cytochrome c release, and mitochondrial size, failed to register significant change. These results reemphasize the remarkable sensitivity of this technique. At higher, lethal concentrations, in the range 1 to 100 nM of vinblastine, the PT response showed dramatic and abrupt changes in magnitude and direction (Fig. 4). In this higher concentration range, conventional assays showed changes in cell size, mitochondrial size, and cytochrome c release into the cytosol, and at a later time-point of 48 h, overt signs of apoptosis including PARP cleavage and loss of cell viability.

These data raise key questions: What are the cellular absorbing structures that are sensitive to drug impact? What is the mechanism of the PT response from such structures? Recently, we have developed the nanocluster model of the PT assay and verified it during the study of nicotine-induced changes in cell metabolism and apoptosis.³⁴ Here we have applied this model for interpretation of antitumor drug action. Briefly, in the PT assay, the cellular response to the drug impact is monitored through drug-induced changes in PT responses from light-absorbing, nonfluorescent endogenous cellular nanoclusters that can be used as natural indicators of the drug's effects. Indeed, many cellular proteins with chromophore groups (e.g., cytochromes) are involved in metabolic sensing pathways that are extremely sensitive to drug action.^{1-3,36} From a diagnostic perspective, most chromophores provide the strongest local absorption in the visible and near-infrared regions (at least 10^3 times higher than background absorption from water, lipids, etc.) with different localization in plasma membrane or in subcellular organelles.^{54,55} Intracellular absorption depends on the size of the absorbing chromophore molecules, their spatial organization, and their ability to create molecular nanoclusters.³⁴

The high-resolution images in the current studies made it possible to determine the similarities of local cellular structure profiles obtained in parallel with PT [Fig. 2(h)] and fluorescent technique in the same cells with selective labeling of mitochondria [Fig. 2(g)] and cytochrome c [Fig. 7(b)]. In addition, the good correlation of the PT spectra of individual local zones in PT images with the conventional spectrum of cytochrome c (not shown, see detail in Ref. 24) confirm that one of the main dominant cellular absorbing components in the spectral range used (530 to 560 nm) is cytochrome c located in mitochondria.⁵⁴ This finding is consistent with data obtained using the PT frequency domain scanning mode.³⁰ Besides, with transmission electron microscopy of cells after exposure with relatively high laser pulse energy (532 nm, 20 J/cm², 12 ns), we observed that a distinctive local photo-

damage in cellular ultrastructure was confined to the mitochondria.

Thus, the basic informative cellular parameter provided by laser PT assay is an absorption coefficient, in particular, of cytochrome c, in mitochondria. In linear mode, the local PT-image amplitude [Figs. 2(d) and 2(h)] is related to local cellular absorption, while the integrated PT response [Fig. 3(a)] is related to average absorption within whole cells. In nonlinear mode, the bubble formation around the local absorbing zone provides information on the level of local absorption through the nonlinear differential PT parameter $\Delta\delta_{NL}$ indicating the probability of bubble-related PT responses as a function of local cellular absorption (e.g., with local absorption increase parameter $\Delta\delta_{NL}$ increase, see details in Ref. 34). We found that rapid measurement of the number of nonlinear PT responses related to bubble formation around local absorbing structures seems to be much more sensitive and accurate to low dose drug impact than measurement of the amplitude of linear PT responses (principle similarity to analogue versus digital techniques).

As we demonstrated, the PT responses are very sensitive to drug-induced changes in local cellular absorption.^{33,34} Indeed, many of the cellular events during drug-cell interaction (e.g., change in metabolism, inactivation of enzymes, or induction of apoptosis and necrosis) are accompanied by changes in local absorption in micro- and nanostructures during their shrinking, swelling, or spatial reorganization. It is interesting that morphological changes during apoptosis- and toxic-related necrosis are completely different.⁵⁶ In particular, during necrosis, the cells and the mitochondria extensively swell with early rupture of the plasma membrane, releasing cytoplasmic contents into the intercellular space. By contrast, during mitochondria-dependent apoptosis (focus of our study) as early events, the cells and mitochondria shrink leading to the hyperdensity of mitochondria ("mitochondrial pyknosis"), but the organelles retain their integrity, and the plasma membrane later develops blebs, but does not rupture. The elongated and dispersed form of mitochondria in control cells changes during apoptosis and they become more spherical and may be clustered around the nucleus forming aggregates with budding-like structures.⁵⁶ During this process, the mitochondrial matrix swells leading to the dominant expansion of the inner membrane that compresses cytochrome c, located between the inner and the outer mitochondrial membranes. Cytochrome c becomes more dense with increased local absorption. Then, the size of the outer membrane may increase and cytochrome c is released from mitochondria. This process is very fast (takes just a few minutes)^{57,58} and drug dose-dependent.³⁴ It is important that mitochondria aggregation precedes cytochrome c release and caspase activation.⁴⁰ As a result, cytochrome c located in mitochondria form punctate nanoclusters, whereas after apoptotic release, cytochrome c is diffuse partly in cytosol [Fig. 7(b)], which is consistent with data published elsewhere (e.g., Refs. 30, 40, 57, and 58). The cell shrinking with cytochrome c release can be considered a sign of early apoptosis because it happens before condensation of nuclear chromatin and membrane blebbing.⁵⁶ The slight shrinking phenomena may also occur during natural reversible metabolic cell responses to drug impact at low drug doses^{15,34} compared to much higher doses required to induce apoptosis.⁵⁶⁻⁵⁸

Thus, according to the described phenomenological model of PT assay, the qualitative relationship between drug action and nonlinear PT responses through parameter $\Delta\delta_{NL}$ is as follows: (1) drug-induced change of mitochondria sizes, (2) change in local concentration of cytochrome c, (3) change in local absorption associated with cytochrome c, (4) change in laser-induced local temperature, (5) change in linear PT response amplitude and the probability of nonlinear PT response. A quantitative relationship can be established based on comparison of cell response to different drug concentration assessed in parallel with PT assay through parameters $\Delta\delta_{NL}$ (Fig. 4) and conventional assays (Fig. 5). These and our other results^{33,34} indicate that the PT assay can be used to conveniently and rapidly monitor and quantitate toxic and apoptotic effects. Toxic effects are accompanied by gradual mitochondria swelling that leads to a gradual slow decrease of $\Delta\delta_{NL}$ having a negative sign. On the contrary, the early apoptotic effects are accompanied by mitochondrial shrinking with compression of cytochrome c, which can be detected through an increase of parameter $\Delta\delta_{NL}$ having a positive sign.³⁴ At a later stage, cytochrome c release leads to a very sharp and profound decrease in $\Delta\delta_{NL}$, having a positive sign before and a negative sign after accomplishing this process. The simultaneous appearance of toxic and apoptotic phenomena leads to more complicated behavior of $\Delta\delta_{NL}$, such as toxicity-related gradual dropping of negative $\Delta\delta_{NL}$ with the appearance of sharp apoptotic-related changes in the concentration range 10 to 50 nM (Fig. 4).

Thus, necrotic (toxic) mitochondria swelling and apoptotic-related release of cytochrome c lead to decreased linear and nonlinear PT parameters. Distinguishing two different cell death processes (apoptosis or necrosis), in this case, with PT technique, may require measuring PT parameters for at least two different drug concentrations, taking into account the different behavior of the parameter $\Delta\delta_{NL}$ described above, including its changed sign. For example, in linear mode, an increase in integrated PT response from whole apoptotic cells and local PT image amplitude compared to control, on average, for early apoptosis was 2 to 3 times and 3 to 5 times, respectively, while a decrease in the same parameter for necrotic cells reached 2 to 3 and 5 to 10 times, respectively. Because shrunken apoptotic and swollen necrotic cells are different sizes (up to 1.5 to 2 times), measuring the PT response tail, which is related to cell size, is another way to discriminate such cells without their imaging.⁵³ Recently, we discovered that in two-beam (pump-probe) PT schematics (Fig. 1), the temporal fluctuation of the probe beam, even without the pump laser pulse, is very sensitive to functional states of single cells, giving an additional method to distinguish apoptotic or necrotic cells with increases and decreases in intracellular traffic, respectively, compared to normal cells.⁵⁹

Another question is how to distinguish metabolic- and apoptotic-related shrinking phenomena, which both lead to an increase in the positive component of $\Delta\delta_{NL}$. According to our previous³⁴ and current findings, the first process is very gradual in a large concentration range from low to moderate concentrations, while apoptotic-related shrinking takes place at higher concentrations with higher increases in rate in a narrower concentration range. Our data with monitoring of PT

responses from different cell types with the same impact (e.g., nicotine³⁴) as well as from the same cell type with different antitumor drugs³³ confirms the described qualitative behavior of parameters $\Delta\delta_{NL}$ and its similarity for different drugs and cells with quantitative differences in those drug doses that induce similar PT responses.

Much of the previous work with conventional assays has focused mostly on lethal drug concentrations that lead to cell death by apoptosis or necrosis.¹⁻¹¹ However, the observation of more subtle drug effects has been hampered by the lack of an appropriate assay sensitive enough to detect the effects of drug concentrations as low as the PT assay enables. While these dramatic changes in cell organization may be responsible for the PT response generated at high drug doses, the exact source of the PT response at low drug concentrations remains uncertain. Low drug concentrations could alter certain aspects of cell structure or function in ways that are sensitive to a PT response but not measurable using conventional assays, or perhaps simply the presence of a drug within the cell provides a signal. In particular, for 24-h vinblastine incubation, we observed only very small, not statistically significant, increases in the positive component $\Delta\delta_{NL}$ at a dose of 10^{-9} nM with the dominant negative component of $\Delta\delta_{NL}$ at higher concentration (Fig. 4). At 1-h incubation, we observed a gradual, more profound increase in the positive component of $\Delta\delta_{NL}$ in the range 10^{-1} to 10 nM and then its gradual decrease in the range 10 to 10^2 nM with no sign change (not shown). In previous studies with a 24-h incubation with the drug paclitaxel (taxol), we also observed a more profound increase in the positive component of $\Delta\delta_{NL}$ in the range of 10^{-9} to 10^{-6} nM, which is associated with metabolic response at low drug concentration with further shift of the negative component at higher concentration.³³ At low vinblastine concentrations, the mechanism of the PT response may be related to changes (e.g., reversible mitochondria swelling) that are undetectable by conventional means. This mechanism might be related to vinblastine-induced modification of microtubules as main cytoskeletal elements, which regulate the distribution of mitochondria in the cells and its morphology. The high sensitivity of PT technique at low concentration range is related with the use of bubble formation phenomena as a super-sensitive indicator of drug-induced changes in local absorption. As we have shown,^{33,34} laser-induced temperature is proportional to the inverse cube of target size (i.e., a decrease in size of 5% leads to an increase in temperature of 15%). When initial laser-induced temperature is close to the bubble formation threshold, for instance, 10% below this threshold, even slight mitochondria shrinking of 5% (which corresponds to change of a mitochondria size of 5 to 15 nm for mitochondria with typical size of 0.1 to 0.5 μ m) leads to sudden bubble formation easily detectable with the PT technique. According to the principle of PT microscopy beyond the diffraction limit,^{24,44} PT detection and especially, visualization, expanded above the diffraction limit bubble provides information of nanoscale absorbing target sizes with a diffraction-limited optical technique. In particular, we demonstrated a relation of nonlinear PT response amplitude and width with average nanocluster sizes at fixed laser pulse energy allowing the determination of these sizes up to 20 nm, if not less.⁶⁰ With high numerical aperture of the microscope

objective, PT technique enables the detection of even single nanobubbles with a size below the diffraction limit.^{44,53} According to the discussion, the PT assay may serve as a highly sensitive indicator of morphological changes at the subcellular level undetectable with conventional microscopy (e.g., change of nanoscale target such as mitochondria size on just 10 to 30 nm). The cell size parameter, which was accurately measured by conventional transmitted light microscopy, changed even at very low drug concentrations (Fig. 8). Because the PT technique is sensitive to changes in internal cellular structures rather than to the overall cell size,³⁴ these data suggest that there is a relationship between these internal structures measured by the PT method and overall cell dimension.

Multidrug-resistant KB-V1 cells, which are unaffected by vinblastine due to a lack of intracellular drug accumulation, do not generate a PT response (Fig. 5). This result provides additional compelling evidence that the PT response is due to the presence of a drug internally. Although we provide reasons that in the spectral range used, the dominant cellular local absorption is determined by mitochondrial cytochrome c, potential contribution in PT response of other cytochromes and influence of membrane plasma proteins, for example, porphyrin-like components⁶¹ requires further detailed study in broad spectral range of 415 to 2300 nm available in the new PT flow cytometer.³⁶ The nanocluster model of the PT assay is applicable also to membrane plasma proteins because cell shrinking leads to decreased distance between molecular absorbing clusters on the membrane leading to increased local absorption.

5 Conclusion

In conclusion, we have demonstrated for the first time the capability of the new high-resolution PT technique, with an extremely high degree of sensitivity, to detect an intracellular antitumor drug in a broad, dynamic concentration range, with threshold sensitivity of 10^{-7} nM, with an acquisition time of around 3 to 5 min, and with no requirement for scanning, fluorescent labeling, or conventional staining. The PT technique is rapid because the assay is responsive to immediate effects of the drugs, whereas conventional viability assays rely on measurement of end points that may take several days to manifest. These data are also the most highly resolved images documented to date with the time-resolved PT technique and therefore represent a significant improvement not only over conventional imaging but also over previously described PT techniques.^{25-37,46,47} We anticipate that this assay may serve as the basis for an automated throughput screening system that is (1) low cost, (2) rapid (minutes), (3) robust, (4) informative (several diagnostic parameters), (5) universal, and has (6) having potential for use in flow cytometry mode.^{36,52,53} This assay also has a potential clinical application to test chemosensitivity of tumor samples and to provide fast feedback control for optimizing individualized cancer treatment strategies. The PT method could potentially be used to indicate the presence of a drug at very low concentrations within different cell types of a tumor. PT response behavior at low and high drug doses could potentially predict the toxicity of chemotherapeutic drugs, allowing adjustment to effective but tolerable doses.

Acknowledgments

This work was supported by National Cancer Institute Grants No. CA097422 (to V. P. Z.), CA075577 (to T. C. C.), and CA010982 (to T. C. C.), and in part by the National Institute of Biomedical Imaging and Bioengineering (Grants No. EB 000873 and EB005123) (to V. P. Z.).

The authors thank Dr. Dmitri O. Lapotko for his help in the development of the first PT microscope prototype that was further significantly modified in V. P. Z.'s laboratory with the introduction of new PT thermolens imaging. We thank Scott Ferguson for his assistance with laser measurements.

References

1. C. D. Klaassen, *Toxicology: The Basic Science of Poisons*, 5th ed., Casarett and Doulls, Eds., McGraw-Hill, New York (1996).
2. K. Horakova, "The use of cell culture systems for the assessment of general cellular toxicity and to detect the nature and location of free radical damage," *Gen. Physiol. Biophys.* **18**, 63-69 (1999).
3. J. M. Frazier, "In vitro models for toxicological research and testing," *Toxicol. Lett.* **68**(1-2), 73-90 (1993).
4. M. D. Enger, "Cellular toxicology," *Rev. Environ. Contam. Toxicol.* **102**, 79-115 (1988).
5. J. C. Davila, R. J. Rodriguez, R. B. Melchert, and D. Acosta, Jr., "Predictive value of in vitro model systems in toxicology," *Annu. Rev. Pharmacol. Toxicol.* **38**, 63-96 (1998).
6. T. R. Dunkern and W. Mueller-Klieser, "Quantification of apoptosis induction by doxorubicin in three types of human mammary carcinoma spheroids," *Anticancer Res.* **19**(4B), 3141-3146 (1999).
7. I. A. Cree, C. M. Kurbacher, M. Untch, L. A. Sutherland, E. M. Hunter, A. M. Subedi, E. A. James, J. A. Dewar, P. E. Preece, P. E. Andreotti, and H. W. Bruckner, "Correlation of the clinical response to chemotherapy in breast cancer with ex vivo chemosensitivity," *Anti-Cancer Drugs* **7**(6), 630-635 (1996).
8. D. S. Waldenmaier, A. Babarina, and F. C. Kischkel, "Rapid in vitro chemosensitivity analysis lines," *Toxicol. Appl. Pharmacol.* **192**(3), 237-245 (2003).
9. D. Shimizu, T. Ishikawa, Y. Ishikawa, S. Togo, Y. Hayasizaki, Y. Okazaki, and H. Shimada, "Current progress in the prediction of chemosensitivity for breast cancer," *Breast Cancer* **11**, 42-48 (2004).
10. M. Untch, A. Untch, B. U. Sevin, R. Angioli, J. P. Perras, O. Koechli, and H. E. Averette, "Comparison of paclitaxel and docetaxel (Taxotere) in gynecologic and breast cancer cell lines with ATP-cell viability assay," *Anti-Cancer Drugs* **5**(1), 24-30 (1994).
11. J. M. Frazier, "A theoretical model for simulating the outcome of mechanism based in vitro toxicity testing strategies," *Toxicol. In Vitro* **18**, 171-178 (2004).
12. R. I. Freshney, Ed., *Animal Cell Culture: A Practical Approach*, p. 329, IRL Press, Oxford, UK (1992).
13. O. Tounekti, J. Belehradek, Jr., and L. M. Mir, "Relationships between DNA fragmentation, chromatin condensation, and changes in flow cytometry profiles detected during apoptosis," *Exp. Cell Res.* **45**, 567-578 (1995).
14. I. Szundi, G. L. Liao, and O. Einarsdottir, "Near-infrared time-resolved optical absorption studies of the reaction of fully reduced cytochrome c oxidase with dioxygen," *Biochemistry* **40**, 2332-2339 (2001).
15. D. G. Weiss, "Videomicroscopic measurements in living cells: Dynamic determination of multiple end points for in vitro toxicology," *Mol. Toxicol.* **1**, 465-488 (1987).
16. W. Maile, T. Lindl, and D. G. Weiss, "New methods for cytotoxicity testing: Quantitative video microscopy of intracellular motion and mitochondria-specific fluorescence," *Mol. Toxicol.* **1**, 427-437 (1987).
17. J. Slavik, *Fluorescence Microscopy and Fluorescent Probes*, Plenum Press, New York, London (1996).
18. J. B. Pawley, Ed., *Handbook of Biological Confocal Microscopy*, 2nd ed., Plenum Press, New York (1995).
19. P. L. Johnson, W. Smith, and S. B. Knisley, "Errors caused by combination of Di-4 ANEPPS and Fluo 3/4 for measurements of transmembrane potentials and intracellular calcium," *Ann. Biomed. Eng.* **24**(4), 563-571 (1999).

20. A. M. Blackwood, G. A. Sagnella, N. D. Markandu, and G. A. MacGregor, "Problems associated with using Fura-2 to measure free intracellular calcium concentrations in human red blood cells," *J. Hum. Hypertens.* **11**, 601–604 (1997).
21. N. Unzubajakava, A. Lenferrink, Y. Kraan, G. Vremsen, J. Greve, and C. Otto, "Nonresonant confocal raman imaging of DNA and protein distribution in apoptotic cells," *Biophys. J.* **84**, 3968–3981 (2003).
22. N. N. Boustany, R. Drezek, and N. V. Thakor, "Calcium-induced alteration in mitochondrial morphology quantified *in situ* with optical scatter imaging," *Biophys. J.* **83**(3), 1691–1700 (2002).
23. V. P. Zharov and V. S. Letokhov, *Laser Optoacoustic Spectroscopy*, Vol. **37**, Springer-Verlag, Heidelberg (1986).
24. V. P. Zharov and D. O. Lapotko, "Photothermal imaging of nanoparticles and cells (review)," *IEEE J. Sel. Top. Quantum Electron.* **11**, 733–751 (2005).
25. M. Tokeshi, M. Uchida, A. Hibara, T. Sawada, and T. Kitamori, "Determination of suboctomole amounts of nonfluorescent molecules using a thermal lens microscope: Subsingle-molecule determination," *Anal. Chem.* **73**, 2112–2116 (2001).
26. M. M. Shibata, T. Kitamori, and T. Sawada, "Application of coaxial beam photothermal microscopy to analysis of a single biological cell in water," *Anal. Chim. Acta* **299**, 343–347 (1995).
27. D. O. Lapotko, T. R. Romanovskaya, G. Kutchinsky, and V. P. Zharov, "Photothermal studies of modulating effect of photoactivated chlorine on interaction of blood cells with bacteria," *Cytometry* **37**, 320–326 (1999).
28. D. O. Lapotko, V. P. Zharov, T. R. Romanovskaya, and G. S. Kuchinskii, "Investigation of the influence of the photodynamic effect on micro-organisms using the laser photothermal cytometry method," *Quantum Electron.* **29**(12), 1060–1065 (1999).
29. D. O. Lapotko, T. R. Romanovskaya, and V. P. Zharov, "Photothermal images of live cells in presence of drug," *J. Biomed. Opt.* **7**, 425–434 (2002).
30. E. Tamaki, K. Sato, M. Tokeshi, M. Aihara, and T. Kitamori, "Single-cell analysis via scanning thermal lens microscope with a microchip: Direct monitoring of cytochrome c distribution during apoptosis process," *Anal. Chem.* **74**, 1560–1564 (2002).
31. V. Galitovskiy, P. Chowdhury, and V. P. Zharov, "Photothermal detection of nicotine-induced apoptotic effects in pancreatic cancer cells," *Life Sci.* **75**, 2677–2687 (2004).
32. D. O. Lapotko, "Monitoring of apoptosis in intact single cells with photothermal microscope," *Cytometry* **58**, 111–119 (2004).
33. V. Zharov, V. Galitovskiy, P. Chowdhury, and T. C. Chambers, "Photothermal evaluation of the influence of nicotine, antitumor drugs, and gamma radiation on cellular absorbing structures," *Proc. SPIE* **5329**, 135–144 (2004).
34. V. P. Zharov, V. Galitovskiy, and P. Chowdhury, "Nanocluster model of photothermal assay: Application for high-sensitive monitoring of nicotine-induced changes in metabolism, apoptosis and necrosis at a cellular level," *J. Biomed. Opt.* **10**, 44011 (2005).
35. V. P. Zharov, M. Viegas, and L. Soderberg, "Biological detection of low radiation doses with integrated photothermal assay," *Proc. SPIE* **5697**, 271–281 (2005).
36. V. P. Zharov, E. I. Galanzha, and V. V. Tuchin, "*In vivo* photothermal flow cytometry: Imaging and detection of individual cells in blood and lymph flow (review/prospect)," *J. Cell. Biochem.* **97**, 916–932 (2006).
37. V. Zharov, V. Galitovskiy, and M. Viegas, "Photothermal detection of local thermal effects during selective nanophotothermolysis," *Appl. Phys. Lett.* **83**, 4897–4899 (2003).
38. V. P. Zharov, J. W. Kim, M. Everts, and D. T. Curiel, "Self-assembling nanoclusters in living systems: Application for integrated photothermal nanodiagnostics and therapy (review)," *J. Nanomedicine* **1**, 326–345 (2005).
39. A. H. Wyllie, "The biology of cell death in tumors," *Anticancer Res.* **5**, 131–136 (1985).
40. N. Haga, N. Fujita, and T. Tsuruo, "Mitochondrial aggregation precedes cytochrome c release from mitochondria during apoptosis," *Oncogene* **22**, 5579–5585 (2003).
41. A. Lawen, "Apoptosis—An introduction," *BioEssays* **25**, 888–896 (2003).
42. S. P. Yu and D. W. Choi, "Ions, cell volume, and apoptosis," *Proc. Natl. Acad. Sci. U.S.A.* **97**, 9360–9362 (2000).
43. F. Lang, E. Gulbins, I. Szabo, A. Lepple-Wienhues, S. M. Huber, C. Duranton, K. S. Lang, P. A. Lang, and T. Wieder, "Cell volume and the regulation of apoptotic cell death," *J. Mol. Recognit.* **17**, 473–480 (2004).
44. V. P. Zharov, "Far-field photothermal microscopy beyond the diffraction limit," *Opt. Lett.* **28**, 1314–1316 (2003).
45. V. P. Zharov, K. E. Mercer, E. N. Galitovskaya, and M. S. Smeltzer, "Photothermal nanotherapeutics and nanodiagnostics for selective killing of bacteria targeted with gold nanoparticles," *Biophys. J.* **90**, 619–627 (2006).
46. D. O. Lapotko, T. R. Romanovskaya, A. Shnip, and V. P. Zharov, "Photothermal time-resolved imaging of living cells," *Lasers Surg. Med.* **31**, 53–63 (2002).
47. D. O. Lapotko and V. P. Zharov, "Spectral evaluation of laser-induced cell damage with photothermal microscopy," *Lasers Surg. Med.* **36**, 22–31 (2005).
48. M. Fan, L. Du, A. A. Stone, K. M. Gilbert, and T. C. Chambers, "Modulation of MAP kinases and phosphorylation of Bcl-2 induced by vinblastine represent persistent forms of normal fluctuations at G2/M," *Cancer Res.* **60**, 6403–6407 (2000).
49. M. Fan, M. Goodwin, M. Birrer, and T. C. Chambers, "The JNK/AP-1 pathway is required for efficient apoptosis induced by vinblastine," *Cancer Res.* **61**, 4450–4458 (2001).
50. C. Brantley-Finley, C. S. Lyle, L. Du, M. E. Goodwin, T. Hall, D. Szewo, G. P. Kaushal, and T. C. Chambers, "The JNK, ERK, and p53 pathways play distinct roles in apoptosis mediated by the antitumor agents vinblastine, doxorubicin, and etoposide," *Biochem. Pharmacol.* **66**, 459–469 (2003).
51. D. Shen, C. Carderelli, J. Hwang, M. Cornwell, N. Richert, S. Ishii, I. Pastan, and M. M. Gottesman, "Multiple drug-resistant human KB carcinoma cells independently selected for high-level resistance to colchicine, adriamycin, or vinblastine show changes in expression of specific proteins," *J. Biol. Chem.* **261**, 7762–7770 (1986).
52. V. P. Zharov, E. I. Galanzha, and V. V. Tuchin, "Photothermal image flow cytometry *in vivo*," *Opt. Lett.* **30**, 628–630 (2005).
53. V. P. Zharov, E. I. Galanzha, and V. V. Tuchin, "Integrated photothermal flow cytometry *in vivo*," *J. Biomed. Opt.* **10**, 51502 (2005).
54. P. Nicholl and W. B. Elliot, "The cytochromes," in *Iron Biochemistry and Medicine*, A. Jacobs and M. Woodward, Eds., pp. 221–272, Academic Press, New York (1974).
55. V. S. Letokhov, "Effects of transient local heating of spatially and spectrally heterogeneous biotissue by short laser pulses," *Nuovo Cimento D* **13**, 939–948 (1991).
56. S. Desagher and J.-C. Martinou, "Mitochondria as the central control point of apoptosis," *Trends Cell Biol.* **10**, 369–377 (2000).
57. J. C. Goldstein, N. J. Waterhouse, P. Juin, G. I. Evan, and D. R. Green, "The co-ordinate release of cytochrome c during apoptosis is rapid, complete, and kinetically invariant," *Nat. Cell Biol.* **2**, 156–162 (2000).
58. J. C. Goldstein, C. Muñoz-Pinedo, J. E. Ricci, S. Adams, A. Kelekar, M. Schuler, R. Tsien, and D. R. Green, "Cytochrome c is released during apoptosis in a single step," *Cell Death Differ.* **12**, 453–462 (2005).
59. V. P. Zharov, Y. A. Menyaev, E. V. Shashkov, E. I. Galanzha, B. N. Khlebtsov, A. V. Scheludko, D. A. Zimnyakov, and V. V. Tuchin, "Fluctuation of probe beam in thermolens schematics as potential indicator of cell metabolism, apoptosis, necrosis and laser impact," *Proc. SPIE* **6085**, 10–21 (2006).
60. V. P. Zharov, R. R. Letfullin, and E. Galitovskaya, "Microbubbles-overlapping mode for laser killing of cancer cells with absorbing nanoparticle clusters," *J. Phys. D* **38**, 2571–2581 (2005).
61. G. Y. Fraikin, M. G. Strakhovskaya, and A. B. Rubin, "The role of membrane-bound porphyrin-type compound as endogenous sensitizer in photodynamic damage to yeast plasma membranes," *J. Photochem. Photobiol., B* **34**, 129–135 (1996).